Research article

Guiqiang Liu, Yi Liu, Li Tang, Xiaoshan Liu, Guolan Fu and Zhengqi Liu*

# Semiconductor-enhanced Raman scattering sensors via quasi-three-dimensional Au/Si/Au structures

https://doi.org/10.1515/nanoph-2019-0078
Received March 7, 2019; revised April 27, 2019; accepted May 1, 2019

**Abstract:** We present a feasible way to strongly enhance Raman signals via introducing an ultra-thin dielectric film in the dual-layer plasmonic hotspots structure, which forms a quasi-three-dimensional structure. The Raman intensity was obtained with an enhancement factor of 735% for the dual-layer metal structure buffered with an ultra-thin silicon film. Moreover, the silicon layer based surface-enhanced Raman scattering (SERS) substrate provided a Raman signal two to five times larger than that of the silica buffered substrate. These distinct responses confirm that the ultra-thin high-index semiconductor film has the capability of additionally enhancing Raman scattering. Otherwise, the upper and lower metal clusters can support multiple kinds of plasmonic resonances, which produce a remarkable physical enhancement of the Raman signals. Besides these impressive optical properties, the substrates have prominent advantages on structural features, since the fabrication process can be fulfilled simply, suggesting a feasible way for a large-area and low-cost SERS platform. The findings may pave an avenue to achieve insights on the dielectric enhanced Raman scattering and hold potential applications in optoelectronics, such as environmental and health sensors.

**Keywords:** hot spots; plasmonics; quasi-three-dimensional; semiconductor; surface-enhanced Raman scattering.

***Corresponding author: Zhengqi Liu,** Jiangxi Key Laboratory of Nanomaterials and Sensors, Provincial Key Laboratory of Optoelectronic and Telecommunication, College of Physics Communication and Electronics, Jiangxi Normal University, Nanchang 330022, China, e-mail: zliu@jxnu.edu.cn, lzhq86025@163.com. https://orcid.org/0000-0002-0087-8871
**Guiqiang Liu, Yi Liu, Li Tang, Xiaoshan Liu and Guolan Fu:** College of Physics Communication and Electronics, Jiangxi Normal University, Nanchang 330022, China

## 1 Introduction

Since 1974, the enhanced Raman scattering effect has attracted great consideration based on the pioneering discovery by Fleischmann et al. [1]. Milestone demonstrations by Jeanmaire and Van Duyne [2] and Xu et al. [3] finally led to an exciting area of surface-enhanced Raman scattering (SERS). After about 40 years of growth, SERS has been implemented widely by a broad scientific and technology research community for multidisciplinary fields such as photonics and nano-optics, solid-state physics and surface science, biotechnology and analytic chemistry [4]. As regards chemical detection and bio-sensing applications, SERS has become a powerful technique, since it combines the capability of a molecular finger-print with ultra-high and even single-molecular detection sensitivity [3, 5, 6], as well as the option for non-destructive real-time label-free analyses *in situ* [7, 8]. These analyzing and measurement features are unique and cannot be achieved with other spectroscopic techniques. Raman scattering, as one of the surface-enhanced spectroscopies, is a process where the photons are inelastically scattered via the vibrational levels of an emitter/analyte. Noble metal structures are the conventional substrates for SERS, which can lead to strong enhancement of the Raman signal for the analyte [9, 10]. The extremely amplified Raman scattering intensity and the corresponding related low limit of detection can enable trace detection and analysis of significantly important molecules and materials, including explosives, pesticides, and biomarkers for the protection and preservation of the health of humans [11–13].

Metal nanoparticles or nanostructures can produce strong plasmonic resonances due to the electronic oscillations driven by the incident electric field. These plasmonic metal materials are able to confine the electromagnetic (EM) field in the sub-wavelength region and provide an extremely enhanced plasmonic field. Particularly, the well known “hot spot” can be excited when the resonant EM field is localized at the interparticle spaces and/or near the sharp tips or corners of the metal particles [14–19],

which is of great scientific interest and has led to a few impressive applications including SERS and bio-sensing. For metal nanocubes, plasmonic hot spots can be formed between adjacent nanocubes in the configurations of face-to-face, edge-to-edge, and face-to-edge. These different coupling geometries of the nanocubes lead to distinct Raman signal enhancement [20]. Generally, sharp protrusions in the metal nanostructures can produce plasmonic hot spots. For instance, metal nanoparticle aggregates with various structures such as triangles [21], disks [22] and rods [23] have been demonstrated to produce hot spots. Ordered nanoparticles arrays can also be prepared to produce strong EM field enhancement for SERS measurements based on the self-assembly methods and nanofabrication techniques [24, 25]. Currently, by using host-guest chemistry, single molecules are observed to be positioned in a plasmonic nanojunction, which can provide EM hot spots and therefore enhance the SERS signals [26]. A novel plasmonic heterodimer nanostructure fabricated by the conjugation of individual Au@Ag core-shell nanocubes and varisized gold nanospheres via the biotin-streptavidin interaction from the ensemble to the single-assembly level has been demonstrated to produce a controllable self-assembled hot spot, which was then utilized for SERS detection [27]. Based on the spatially combined nanocube and nanosphere cells, different types of heterodimers can be achieved, which can provide an alternative way to tune the SERS detection and produce distinct SERS intensity and enhancement factors.

Besides the extensive study on the building of EM hot spots by different structural geometries, shell-isolated plasmonic structures have also been developed in these years to provide efficient SERS measurement. Shell-isolated gold nanoparticles with ultra-thin silica or alumina shells have been chemically synthesized [28]. The ultrathin coating can keep the metal nanoparticles away from agglomeration. The Raman vibrational bands or the chemical signal of the molecules can be strongly enhanced due to the strong EM field transferred to the shell surface by the metal nanoparticles. The jointly enhanced Raman signal contributed by the metal nanoparticles array, similarly to thousands of tip-enhanced Raman spectroscopy tips, was observed to be about two or three orders of magnitude higher than that for a single tip [28]. An enhanced Raman signal was also demonstrated for the silver particles based substrate by coating with a 1 nm diamond-like carbon film via a precise technique [29]. The enhancement factor of the SERS was nearly twice that of the uncoated substrate. Recently, a sandwich-structured SERS substrate produced by integrating gold particles and an electron beam lithography-fabricated silver holes array separated by a single layer of graphene was reported [30]. The chemical enhancement arising from the graphene-molecule interaction, or the so-called charge transfer between graphene and molecules, together with the localized EM fields in the nanogap sandwich structure, provided a strongly enhanced Raman signal. Although many great efforts have been made in efficient SERS by physical or chemical methods for the substrates, the feasible way for large-area, low requirement of fabrication techniques, as well a large spatial distribution density of EM hot spots, has long been pursued.

Recently, SERS on semiconductor materials has also been explored [31–33]. Semiconductor resonators have been demonstrated with strong electron and magnetic resonances [34–37]. Plasmon-like hot spots [38, 39] and EM-induced transparency [40] and nonlinear optics [41] have been theoretically proposed and experimentally demonstrated. Although there are no free electrons in the semiconductors, the electron-hole pair or the so-called exciton can be generated under external illumination. This can then produce strong charge-transfer or resonant coupling with adjacent metals or molecules. Based on the all-dielectric nanoantenna, SERS of a molecular monolayer has been observed [42]. However, the enhancement factor of SERS signals for the silicon dimers is nearly three orders of magnitude less than that of the gold substrate, since gold can enhance the inelastic scattering of light much stronger than dielectrics. These results indicate that, in principle, for SERS enhancement applications, metals still play a superior role over low-loss dielectrics. By combining a common metal particles substrate with a photo-activated semiconductor, a novel photo-induced SERS enhancement was observed [12], whereby pre-irradiation of the semiconductor, such as titanium oxide, enabled strong Raman enhancement at the particle sites, showing additional increasing sensitivity beyond the normal SERS effect. The additional enhancement factor by using the photo-inducing process is about two in comparison with that of convenient metal particles based SERS substrates. These findings provide a new insight on the mechanism for SERS. Nevertheless, there is still the virgin land on the forward of the metal-semiconductor incorporated SERS substrates.

In this work, we focused on a feasible way to build a simple and universal SERS substrate scheme by combining the plasmonic metal structure and the dielectric film. In contrast to the precisely designed and fabricated metal SERS substrates by the electron beam or focused ion beam lithography or other chemical synthesis methods, only a physical sputtering deposition and a relatively low temperature annealing treatment are needed. The dielectric

films of the semiconductor or insulator are directly deposited onto the metal substrate. A triple-layer of a metal-dielectric-metal structure was proposed as the system for the study on SERS behaviors with different dielectric materials and thicknesses. It was observed that the gold-silicon-gold incorporated system could produce nearly a 735% enhancement effect in comparison with that of the gold SERS substrate without the silicon buffer layer. As for the insulator separated substrate, the optimized SERS enhancement factor was about 196%. These features confirm the great contributions for Raman scattering by the high-index semiconductor. The findings can pave new ways to develop the science on SERS and produce new insights into how to further improve the Raman detection based on the existing technology.

## 2 Materials and methods

The detailed process was a four-step operation. The first step was to deposit a 20-nm-thick gold (Au) film on a piece of silicon wafer. Then, a relatively low temperature of 220°C (~493 K) was used during a 30-min anneal treatment for the Au film. After this procedure, the Au clusters film was obtained. A dielectric film with a certain thickness value was then deposited on to the Au clusters film and the other 20-nm-thick Au film was deposited. The same anneal treatment procedure was used for the Au film, which led to the formation of the top Au clusters and finally completed the fabrication. The same fabrication process was used, but a thinner 8-nm-thick Au film with a lower heat treatment temperature of 190°C (~463 K) was chosen for the dual-layer Au particles structure. The deposition of Au films was under conditions of 20 sccm argon gas, 3.3 Pa and 0.2 A of direct current, which produced an average deposition velocity of 32 nm per min. For the Si film, the deposition conditions were 7 sccm argon gas, 1.0 Pa and 100 W of radio-frequency voltage, which then provided an average deposition velocity of 3 nm per min.

The structural geometry was measured by scanning electron microscopy (SEM) (S3400, Hitachi, Japan). The reflection was measured with a commercial Lambda 750 spectrophotometer. The reflection spectra were normalized by the reflective intensity by the standard mirror. There was a slight oblique angle of ~12° for the reflection measurement.

The samples were immersed in the R6G molecular solution for about 12 h, and then they were rinsed in deionized water to form monolayer analytes on the surface of the structure. In this work, a concentration of $10^{-8}$ mol/l R6G solution was utilized for the SERS detection. A continuous laser source with a wavelength of 514 nm under a relatively low power of 20 μW was used for the Raman scattering excitation. A 100× objective lens was used for the Raman spectrograph by the HR 800 spectrometer (Horiba Scientific, HR Evolution). The integration time was set to be 10 s during the measurement.

Numerical simulation was performed by the three-dimensional finite-difference time-domain method [43]. Dual-film Au star-shape particles were used as the ideal model for the clusters, since the star-shape particles have such structural features as sharp corners and air gaps, which are similar to the Au clusters. The length of each vertice to the center was 0.14 μm. The star-shape particles were packed to a periodic triangular array with a lattice constant of 0.3 μm. These parameters are comparable to the experimental data. The bilayer star-shape particles were sandwiched by a Si layer. The Si layer was 1 nm thick. Moreover, the top and bottom clusters were set to have a spatial separation of $\delta x = \delta y = 20$ nm, which is used to qualitatively fit the experimental phenomenon. Periodic boundary conditions were adopted in both the $x$- and $y$-directions to reproduce the array pattern. Perfectly matched layers were employed in the $z$-direction immediately outside of the structural region. The dielectric constants of the gold and silicon were obtained from the experimental data by Palik [44]. The silica material was set to be dispersionless and the refractive index was 1.45. Under these conditions, we evaluated the electric field distributions in the top and bottom Au clusters, and the middle silicon film.

## 3 Results and discussion

Two distinct kinds of metallic nanostructures were proposed. The first kind of SERS substrate was composed of dual-layer Au clusters with an ultra-thin dielectric buffer film. Figure 1A presents the schematic geometry for the single layer Au clusters. Numerous air slits or gaps and/or holes under the nanometer scale were located randomly in the thin Au film, which eventually led to a porous-like structure. In the following, we want to call this kind of film structure as the Au clusters to highlight the structural characteristics of the single cluster resonator. Figure 1B shows the proposed Au clusters based dual-layer substrate with an ultra-thin dielectric film. In contrast to the single Au clusters layer with densely packed clusters in the two-dimensional plane, the clusters not only exist at the top layer, but also exist at the crossing areas due to the spatially overlapping of the dual-layer clusters. Therefore, a quasi-three-dimensional Au clusters platform was obtained. It is a novel substrate platform for surface-enhanced spectroscopy

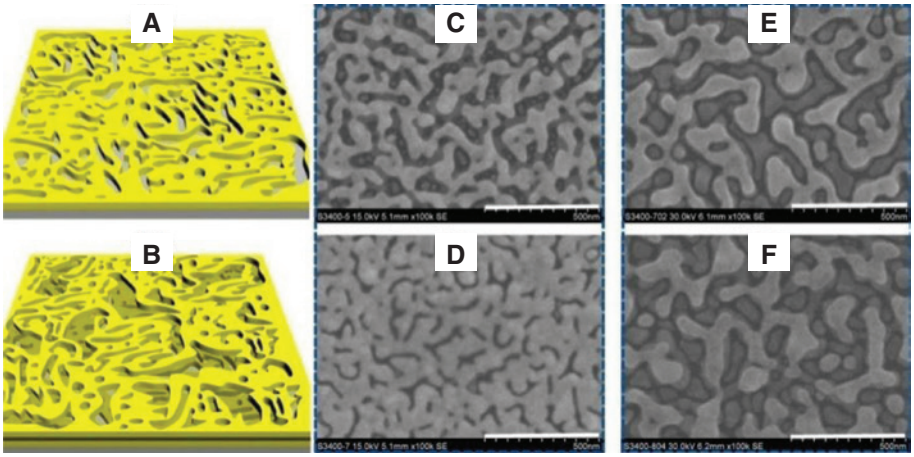


**Figure 1:** Schematics and scanning electron microscopy (SEM) images of the dielectric film sandwiched plasmonic clusters.
Schematic of single layer Au clusters (A) and dual-layer Au clusters with an ultra-thin silicon film (B). (C) (D) Dual-layer Au clusters with a 1 nm silicon and silica film, respectively. (E) (F) Dual-layer Au clusters with a 30 nm silicon and silica film, respectively. The scale bar is 500 nm.

techniques based on these quasi-three-dimensional Au clusters structures, since there are densely packed sharp and nano-gaped metallic tips and corners, which are the sources for plasmon hot spots and can greatly enhance electric field resonant intensity. The spatially distributed plasmonic hot spots in the horizontal plane and the vertical direction indicate a quasi-three-dimensional hot spots bulk structure for this proposed platform. Herein, we put forward a simple and feasible way to realize this novel structure. Based on our previous report [45], we have found out that the geometry features of the thin metal films can be artificially controlled by a moderate thermal treatment. It is feasible to form different nanostructures after a suitable choice of thickness of the film, the temperature and the operating time of thermal annealing.

Figure 1C–F show the SEM images for the dual-layer Au clusters with 1 nm and 30 nm silicon or silica films. Figure 1C and D show the SEM pictures of the dual-layer Au clusters with 1 nm silicon and silica films, respectively. It should be noted that the 1 nm film was an uncontinuous film structure, which was the partially packed cavity coating on the bottom Au nanostructures, since the film thickness was much smaller than the critical thickness of the film formation by the deposition method [46, 47]. Moreover, the ultra-thin film will be further concentrated close to the Au nanostructures after the following heat treatment process [48]. Distinct structural geometries were observed for these two situations. As shown in Figure 1C, the Au clusters with relatively slim branches were indented as the main geometry for the top layer. Moreover, the bottom Au clusters layer was also visible. The Au clusters overlapped with each other and most of them were obviously displaced in the two layers. That is, the top Au clusters layer was not vertically aligned to the bottom layer. The mismatch for these dual-layers is impressive for its following SERS enhancement. Numerous small Au particles were also observed in the nanogap areas. A lot of nanoholes were randomly located in the Au clusters. The nanogaps and nanoholes can not only produce extremely strong local field enhancement, but also provide appropriate places for molecules to be adsorbed. In contrast, it is rather different for the dual-layer Au clusters sandwiched by a $SiO_2$ film. As shown in Figure 1D, the clusters were located densely with each face-to-face. The whole structure was similar to a continuous flat surface with randomly distributed air slits. Owing to the closely packed clusters, the bottom layer was almost covered, without the chance to show the morphology. The distinct geometrical features for these two cases suggest the potential effect on the anneal treatment for the top Au clusters by the high and low index dielectrics. In contrast to the silica, which is a complete insulator, the ultra-thin silicon film had a remarkable optoelectronic effect due to the semi-conductor response. Moreover, in contrast to the bulk semiconductor, the ultra-thin film could have strong quantum effects such as an electron tunneling effect [49, 50], and even partial transformation between the semiconductor and metal [30, 51]. These potential effects directly affect the thermal transformation and dissipation efficiency [52–54], thereby, as for the silicon film sandwiched dual-layer Au clusters, during the heating process for the top Au film, the thermal flow can efficiently transform between the top and bottom Au nanostructures [52–54]. As a result, the top Au film can be strongly affected by the bottom Au clusters. Especially, on the top surface of the bottom clusters, the top clusters film in this close area will

form a strong interaction for the thermal dissipation with the below clusters. As a result, a similar clusters array was reproduced following the template of the bottom Au clusters. As for the situation of the dual-layer with a middle silica film, the thermal transformation was much weaker than that of the above one. Thereby, the top Au film was split randomly due to the thermal instability of the whole film structure. Figure 1E and F show the corresponding SEM images for the situations with 30-nm-thick Si and $SiO_2$ films, respectively. Based on the relatively thick dielectric buffer film, similar structural features such as the large-size clusters and the well-bedded clusters films were observed for these two situations. Nevertheless, some different characteristics were observed between them. For instance, the top layer clusters in Figure 1E almost came in contact together to form a larger spatial size, including the chain length. In contrast, the clusters in Figure 1F were usually smaller and formed shorter chains. As compensation, more particles were observed in the gaps as shown in Figure 1F. These features confirm the different responses for the silicon and silica layers to the formation process for the heat treatment of the thin Au film.

Another kind of plasmonic metal resonant system was proposed with a thin Au film. Figure 2A shows the schematic of randomly packed Au particles after moderate heat treatment of a thin Au film. Based on the four-step procedure, dual-layer Au particles with a thin dielectric buffer layer were obtained, as shown in Figure 2B. It should be noted that the ultra-thin buffer dielectric layer could be discretized to single dielectric pieces based on the geometry feature of the bottom Au particles. Figure 2C shows the SEM image for the 8-nm-thick Au film based structure with a 10-nm-thick Si film after the thermal treatment process. It is observed that densely packed particles were randomly located with a size scale range from ~10 nm to ~50 nm. The middle size level was about 25 nm. Figure 2D presents the SEM image for the system with a 10-nm-thick $SiO_2$ film. Much larger Au particles were obtained. Numerous particles had a size scale of ~40 nm. Simultaneously, the gap distance between adjacent particles was also much wider. These features again confirm that dielectric films with different material characteristics can lead to distinct structural geometries for the Au films during the thermal annealing process. Figure 2E and F show the corresponding SEM images for the system with 30-nm-thick Si and $SiO_2$ films, respectively. A relatively smaller particles distribution can be observed for the system formed by the Si buffer layer.

Figure 3A presents the experimental results of the Au clusters system under different thicknesses of the Si buffer layer. As for the bare Au clusters without a Si layer, the main Raman peaks of the R6G molecules were observed, even if a 10 nmol analytes solution was used to form monolayer molecules on the surface of the Au clusters. This result also confirms that the high detection capability for the Au clusters is due to the strong localized electric field enhancement in the close area by the plasmonic resonances [55–57]. For the proposed Au clusters with an ultra-thin Si buffer layer, the Raman signal was observed to be extremely enhanced. Under the situation of the system with a 1-nm-thick Si layer between the top and the bottom Au clusters films, the SERS spectrum showed a remarkably stronger intensity than that of the Au clusters without the dielectric layer. When the thickness of the Si layer ($t_{si}$)

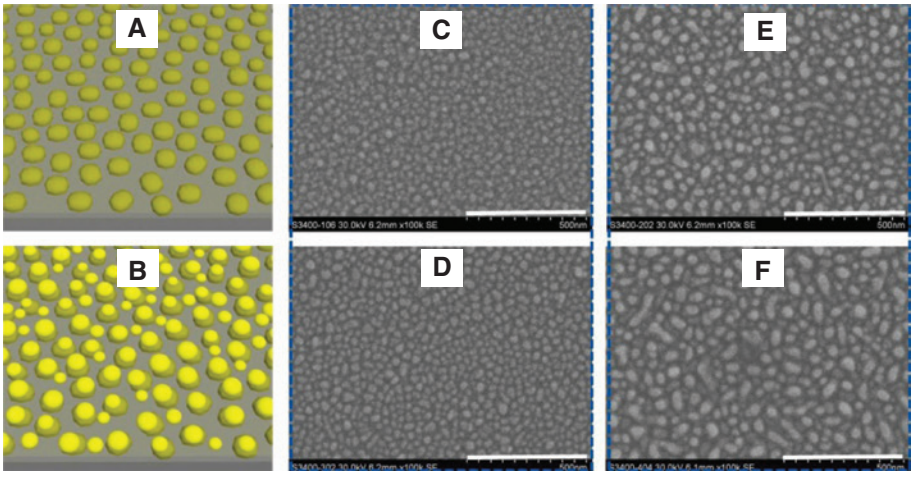


**Figure 2:** Schematics and scanning electron microscopy (SEM) images of the dielectric film sandwiched plasmonic particles.
Schematic of single layer Au particles (A) and dual-layer Au particles with an ultra-thin silicon film (B). (C) (D) Dual-layer Au particles with a 10 nm silicon and silica film, respectively. (E) (F) Dual-layer Au particles with a 30 nm silicon and silica film, respectively. The scale bar is 500 nm.

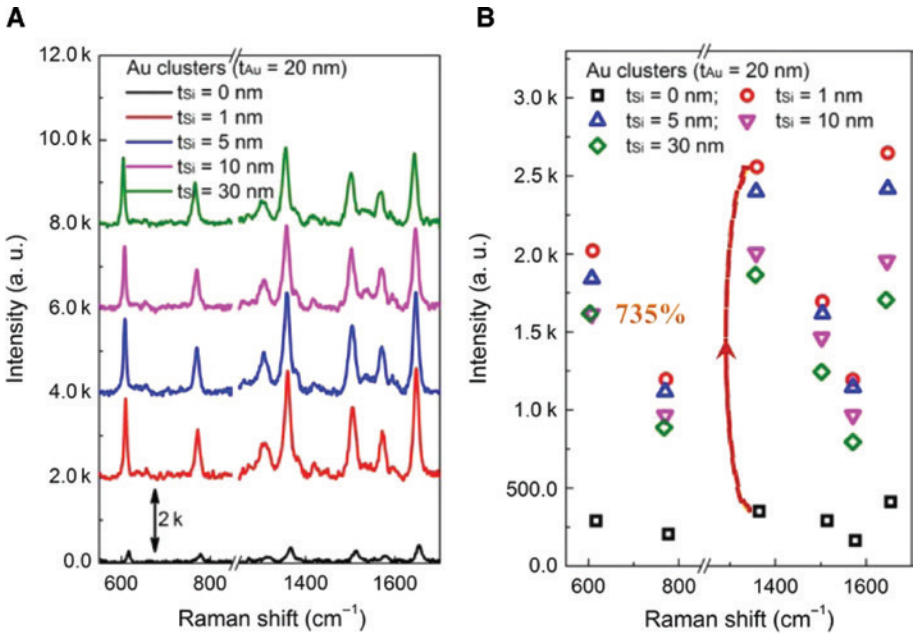


**Figure 3:** Surface-enhanced Raman scattering (SERS) performance for the Au clusters based substrate.
(A) SERS spectral properties of the Au clusters under a tuning thickness of silicon buffer layers. (B) The plotted intensity spectrum of the Raman modes as a function of the silicon layer's thickness. The dashed red arrow indicates a 735% enhancement factor for the 1-nm-thick silicon sandwiched Au clusters to that of the Au clusters structure without the silicon film.

was increased to 5 nm, the SERS intensity values for the characteristic lines were still much larger than that of the referred bare Au clusters. Nevertheless, the Raman curves showed a slightly reduced evolution when the Si layer thickness ($t_{si}$) was increased to 30 nm. To get a clear view of this evolution, the spectral intensity of the main characteristic peaks of the R6G molecule were plotted for these different structures, as shown in Figure 3B. All of the Si layer buffered Au clusters showed a noticeable enhancement in comparison with that of the referred Au clusters. For the main Raman peaks, the 1-nm-thick Si layer was the optimal thickness. The enhancement factor was up to 735% at the Raman peak of 1361 $cm^{-1}$. These results could provide a way for further improving the Raman scattering efficiency by using the ultra-thin Si layer.

Au clusters with a low-index $SiO_2$ buffer layer were investigated for the SERS detection simultaneously. Figure 4A shows the measured Raman scattering results for the system under different thicknesses of the $SiO_2$ layer. For the $SiO_2$ layer insulated Au clusters, the Raman scattering curves only showed slight improvement compared with that of the bare Au clusters. For instance, in contrast to that of the 1-nm-thick Si layer buffered Au clusters with a high enhancement factor, there was an imperceptible improvement for the ultra-thin $SiO_2$ layer sandwiched structure. When the $SiO_2$ layer had a relatively large thickness of about 30 nm, the SERS spectrum showed an observable enhancement. Figure 4B presents the plotted intensity spectrum of the Raman modes as a function of the silica buffer layer's thickness. The spectral enhancement efficiency was relatively weak compared with that of the Si layer sandwiched Au clusters. For instance, only a 196% enhancement factor was obtained for the 30-nm-thick $SiO_2$ layer buffered Au clusters in comparison with that of the bare Au clusters structure. These findings suggest that the low-index dielectric thin films can only provide a slight improvement for the SERS signal intensity.

It is necessary to do further comparison between the high and low-index dielectrics when they are used as the thin film for the plasmonic metal structures since a remarkable different response is observed in the above discussion. Figure 5A shows the Raman signal curves of the 1-nm-thick Si and $SiO_2$ layer buffered Au clusters. The Si layer sandwiched Au clusters showed a much stronger signal intensity than that of the $SiO_2$ layer buffered structure, even if the layer thickness was the same. For instance, the Raman signals at the characteristic lines of 605 $cm^{-1}$, 1356 $cm^{-1}$ and 1644 $cm^{-1}$ realized enhancement factors of 414%, 461% and 527%, respectively. These results directly confirm the impressive Raman scattering enhancement by the high-index dielectric. It should be noted that the Si layer did not only have a difference of the dielectric feature, but also led to a distinct geometry

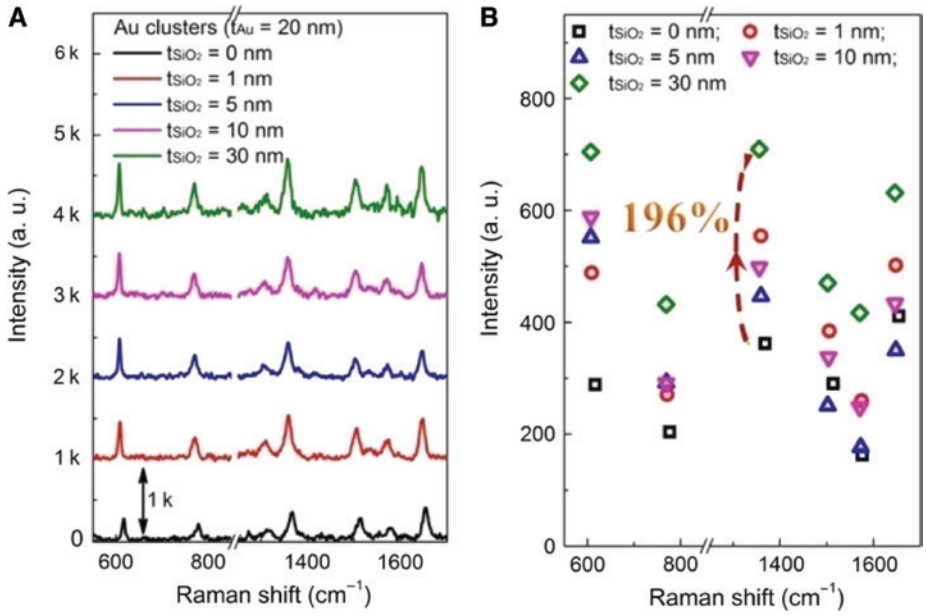


**Figure 4:** Surface-enhanced Raman scattering (SERS) performance for the Au clusters based substrate.
(A) SERS spectral properties of the Au clusters under a tuning thickness of silica buffer layers. (B) The plotted intensity spectrum of the Raman modes as a function of the silica layer's thickness. The dashed red arrow indicates a 196% enhancement factor for the 30-nm-thick $SiO_2$ buffered Au clusters to that of the Au clusters structure without the silica film.

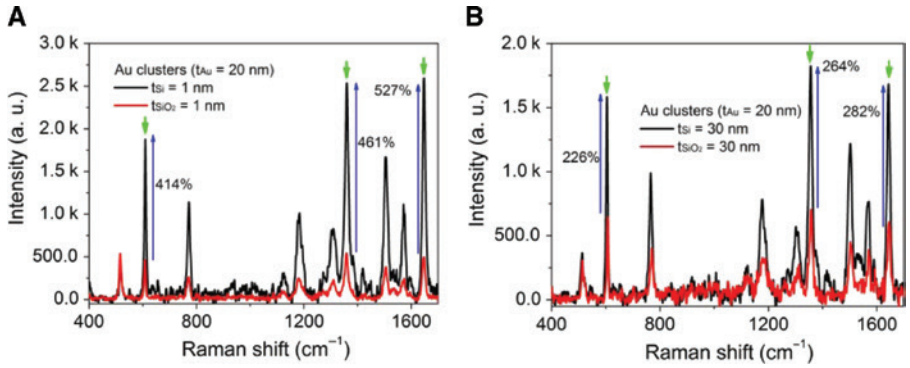


**Figure 5:** Surface-enhanced Raman scattering (SERS) performance for the Au clusters based substrate under different dielectric films.
(A) (B) Comparison of the SERS spectral curves for the Au clusters under the same thicknesses of the Si and $SiO_2$ layers, respectively.

of the Au clusters during the sample preparation. That is, the material feature and the related structural geometry characteristics for the Si layer sandwiched Au clusters are the two main reasons for the excellently enhanced SERS spectrum. The ultra-thin Si layer with a normal thickness of 1 nm is believed to provide strong photonic resonance and simultaneously to provide electron oscillations by the quantum confinement, since the thickness is close to the Bohr radius. As a result, the bilevel Au clusters are not only physically separated by the Si film but also affected by the Si film via the strong electric field oscillations. Localized plasmon resonances and the near-field coupling, and the so-called charge transfer could all be excited in this ultra-thin semiconductor layer sandwiched quasi-three-dimensional metal-semiconductor-metal triple-layer structure. Figure 5B further shows the comparison for the Au clusters formed with 30-nm-thick Si and $SiO_2$ layers. Under such a relatively thick dielectric buffer layer, the Au clusters structures with Si and $SiO_2$ still showed a noticeable difference in the Raman intensity. Enhancement factors of 226%, 264% and 282% of the Raman signals were obtained at the characteristic lines of 605 cm$^{-1}$, 1356 cm$^{-1}$, 1644 cm$^{-1}$, respectively. These results confirm the better Raman scattering for the Si layer based Au clusters. As for the great different Raman scattering responses for the Au/Si/Au and the Au/$SiO_2$/Au clusters, it

is necessary to further discuss the potential contributions by the different morphology features for them. As the SEM images show in Figure 1, the surface morphologies for the ultra-thin films based systems are noticeably different from each other. For instance, with the 1-nm-thick $Si/SiO_2$ film based Au clusters, the morphology patterns are different. As the SEM images show in Figure 1C and D, the 1-nm-thick $SiO_2$ film based structure has many more nanoslits between the adjacent Au clusters, which could produce strong Raman scattering enhancement. However, in fact, the 1-nm-thick Si film based system shows a much larger intensity. Moreover, as regards the 30-nm-thick Si or $SiO_2$ films based systems, the morphologies for these structures are very similar, as shown in Figure 1E and 1F. The Raman scattering still shows an enhancement factor larger than 200% as compared to that of the $SiO_2$ film based system. Furthermore, the difference in the morphology between the Si or $SiO_2$ film based structures is much smaller than that of the Au clusters systems. That is, the morphology part terns for the Au particles with Si or $SiO_2$ interlayers are similar. The spectral intensity curves for the Au particles with Si or $SiO_2$ interlayers are similar to that of the Au clusters, showing a remarkable difference for these different materials, as shown below. These features again indicate that the key contributions to and the great difference between the spectral responses mainly result from the material properties and their related responses. Thereby, the structural morphology is not the key point for the contributions of the distinct responses of the enhanced Raman scattering. Indeed, the material properties of the semiconductor, such as the strong photonic resonances, can produce additional contributions [48–50, 57]. High-index dielectric systems and, in particular, semiconductors, have been tailored to achieve enhanced Raman scattering [42] or related effects [58]. Otherwise, the formation of quasi-three-dimensional clusters can produce efficient EM hotspots, which can provide volume-like enhanced scattering [59] and produce strong contributions. The effect on the extraction of the local field [57, 60] for the plasmonic resonances of the Au clusters by the high-index Si layer could be another contribution to the observed spectral responses.

We studied the SERS response by using Au particles under different conditions. Figure 6A shows the curves for Au particles based structures under different thicknesses of Si layers. As regards the bare Au particles based system, a strong Raman scattering intensity was observed for the characteristic peaks of the analytes, suggesting a high capability for trace detection. This is also the reason why there were many applications on the molecular detection and sensing by using the plasmonic nanoparticles [61], especially for the densely packed particles. The strong local electric field and the plasmon near-field hot spots which exist in the densely distributed metal particles can

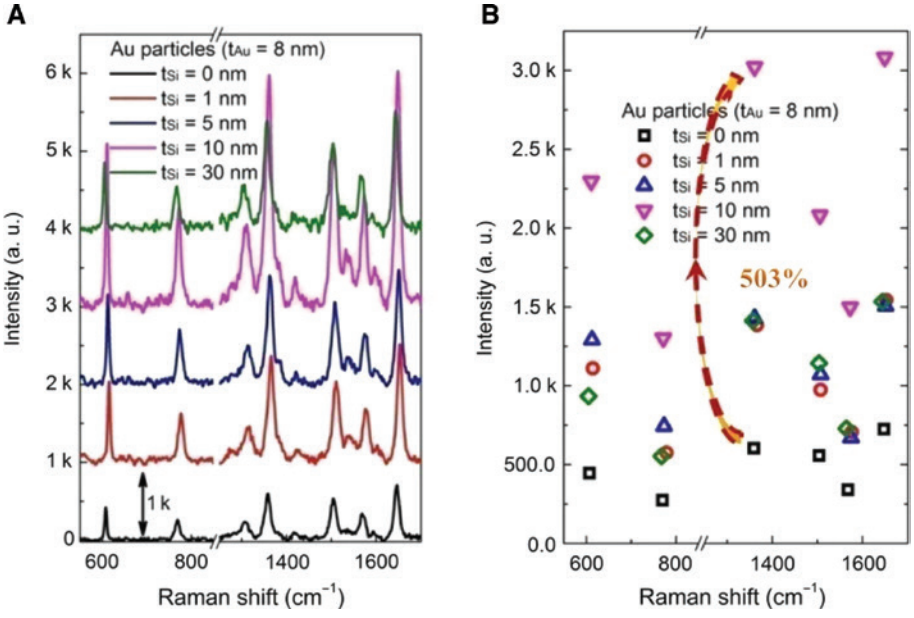


**Figure 6:** Surface-enhanced Raman scattering (SERS) performance for the Au particles based substrate.
(A) SERS spectral properties of the Au particles under a tuning thickness of silicon buffer layers. (B) The plotted intensity spectrum of the Raman modes as a function of the silicon layer's thickness. The dashed red arrow indicates a 503% enhancement factor for the 10-nm-thick silicon buffered Au particles to that of the Au particles structure without the silicon film.

produce an ultra-high detection capability [62–64]. Nevertheless, these investigations were focused on improving the efficiency based on the metal particles themselves. Far less attention was paid to further enhancing the SERS with the help of the external environment. Herein, we combined the common high-dense Au particles with the ultra-thin dielectric layers and then formed a novel SERS substrate. The Raman intensity for the characteristic lines of the Si layer sandwiched Au particles substrates was much stronger than that of the bare Au particles. When the thickness of the Si layer was increased from 1 nm to 10 nm, the Raman scattering intensity showed a continuous rise. The Raman signal was then reduced when the Si layer was as thick as 30 nm. The plotted spectrum for the main Raman characteristic lines under different thicknesses of the Si layer is presented in Figure 6B. The Raman signal for the 10-nm Si layer sandwiched Au particles substrate was much stronger than that of the other situations. In comparison with that of the bare Au particles based substrate, the enhancement factor was up to 503% at the Raman peak of 1361 $cm^{-1}$ for the 10-nm Si layer buffered Au particles substrate. Strong enhancement of the Raman scattering was also observed for other main characteristic peaks. These features suggest that the introduced Si layer with a suitable thickness can not only retain the high-efficiency Raman scattering of the bare Au particles, but can also provide additional enhancement.

Figure 7A presents the Raman intensity evolution for the Au particles based substrates under a tuning thickness of the $SiO_2$ buffer layer. During the increase in the thickness of the silica layer, the Raman spectral curves had a similar intensity to that of the bare Au particles structure. Only a slight enhanced Raman signal was observed when the silica layer was about 10 nm. The Raman intensity then became weak when a thick silica layer was used. Figure 7B shows the plotted spectral intensity of the Raman modes as a function of the silica buffer layer's thickness. For the Raman characteristic peaks, only a small enhancement factor was obtained when the substrate had a 10-nm-thick silica layer. For instance, in comparison with that of the bare Au particles based substrate, the enhancement factor was about 172% at the Raman peak of 1361 $cm^{-1}$ for the 10-nm silica layer buffered Au particles substrate. These results suggest that the low-index silica buffer layer has a relatively weak contribution for improving the SERS.

We further studied the producibility for the proposed system. As shown in Figure 8A, the Raman spectra of the Au clusters with a 1-nm-thick Si interlayer were presented when a continuous measurement was carried out 12 times in the same point. Only slight changes were obtained for the main scattering peaks. Figure 8B shows the spectra of the system after measurements at different points. The spectral intensity had a moderate fluctuation for the main

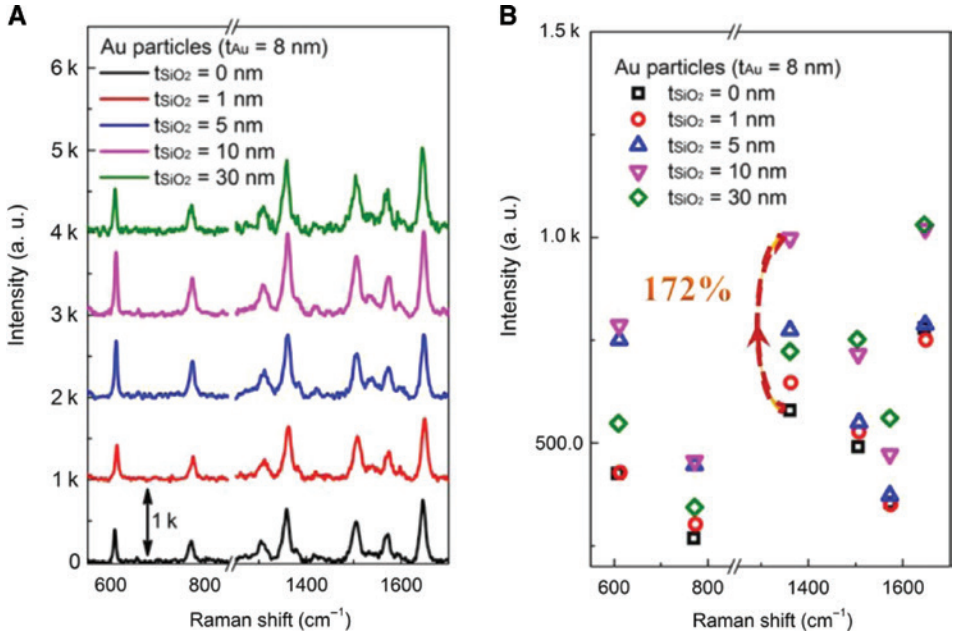


**Figure 7:** Surface-enhanced Raman scattering SERS performance for the Au particles based substrate.
(A) SERS spectral properties of the Au particles under a tuning thickness of silica buffer layers. (B) The plotted intensity spectrum of the Raman modes as a function of the silica layer's thickness. The dashed red arrow indicates a 172% enhancement factor for the 10-nm-thick silica insulated Au particles to that of the Au particles structure without the silica film.

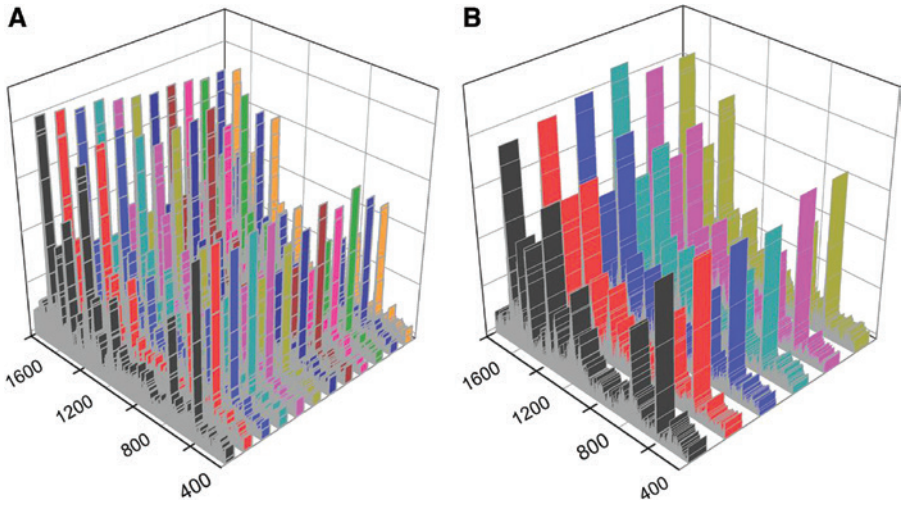


**Figure 8:** (A) (B) Raman spectra of the Au/Si/Au clusters with a 1-nm-thick Si interlayer after continuous measurements for 12 times and the spectra for six different points.

Raman resonant peaks. These features confirm the high producibility and uniformity for the proposed substrate.

Finally, we would like to discuss the mechanism for the observed dielectric film enhanced SERS behaviors, especially for the Si ultra-thin film sandwiched Au clusters. Figure 9A shows the schematic of the intrinsic and potential mechanisms for the ultra-thin Si layer sandwiched Au clusters. For a single layer of the Au clusters, owing to the densely distributed sharp Au corners and nanogaps between the adjacent parts, several kinds of plasmonic resonances can be excited. For instance, the sharp corners or the tips of the Au clusters can produce tip-like plamson local electric field enhancement, the plasmon hotspots [14–19]. Moreover, between the adjacent clusters, the randomly distributed air gaps can lead to the excitation of gap plasmon modes. These gap plasmons occur at the ultra-small area and therefore produce the gap plasmon hotspots [65]. Additionally, as for the clusters themselves, the localized plasmons or the particle plasmons can be excited by these metal nanostructures [66, 67]. When the dual-film Au clusters are combined with an ultra-thin dielectric film, the spatially

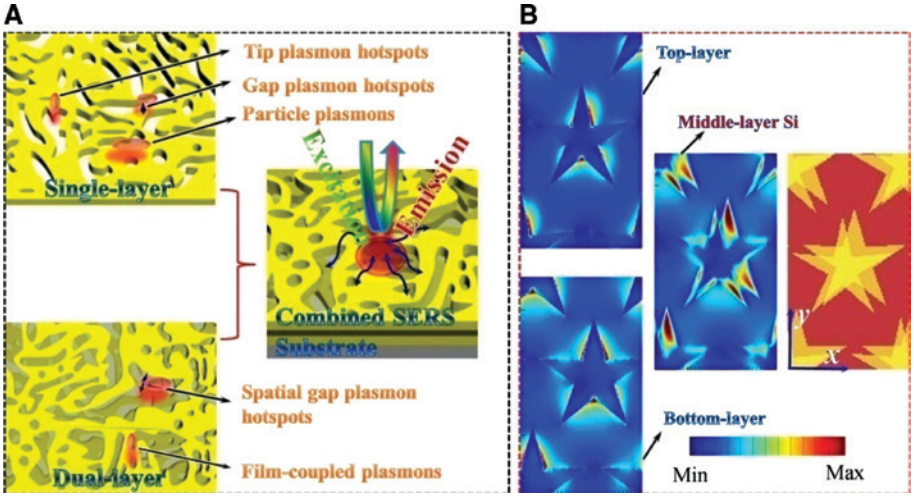


**Figure 9:** Mechanism discussion of the film buffered dual-layer plasmonic clusters.
(A) Schematic of the potential contributions for the enhanced surface-enhanced Raman scattering (SERS). The combined SERS substrate is the efficient cooperation between the multiple plasmon modes and the tip, gap based plasmon hotspots, the film-coupled plasmonic resonances, and other plasmon hotspots by the spatially distributed and displaced clusters and/or their sharp edges and corners.
(B) Calculated local electric field distributions in the top and bottom Au clusters, and the middle Si layer. The schematic of the ideal model is designed as dual-film Au star-shape clusters sandwiched by a Si layer. The top and the bottom clusters have a spatial separation.

distributed metal nanostructures can produce other plasmonic resonant effects. For instance, the gaps can even be formed by the top and bottom clusters, which usually exhibit spatial displacement in the quasi-three-dimensional scale. This structural feature leads to numerous spatial gaps plasmon hotspots, which are distributed in the nanometer scale since the buffer layer is ultra-thin. Between the top and bottom clusters, the plasmons can couple with each other and eventually form the film-coupled plasmons. These plasmonic resonances and coupling effects can strongly enhance the local electric fields and produce higher Raman scattering signals. Similar responses could also be achieved for the silica interlayer based systems. Nevertheless, when a high-index dielectric layer is used, such as the semiconductor Si, the photonic resonances and the intrinsic electrical features can provide additional contributions for the enhanced SERS [12, 37, 42]. The insulator interlayer has poor electronic responses and cannot produce these similar contributions. For instance, the ultra-thin Si film or cavity has been observed to support low-order localized optical resonance and strong EM resonances [68]. In particular, semiconductor nanoresonators have a high density of electrons, which could be excited to interact with other electronic oscillations and could even provide a so-called charge transfer [30, 69–71]. The ultra-thin Si film with a thickness close to the Bohr radius produces plasmon-like responses, which produce efficient coupling and resonant channels for the top and bottom Au nanostructures, leading to the formation of quasi-three-dimensional volume-like Raman scattering substrates. These features can provide other ways to enhance the SERS. Under laser excitation, the monolayer molecules can be coupled and excited by these effects, which provide strong Raman signals. Figure 9B shows the calculated local electric field distributions of an ideal model with dual-layer Au star-shape clusters, separated with a 1-nm-thick Si layer. In order to fit the actual situation, the dual-layer clusters were spatially displaced as the schematic diagram shown in Figure 9B. Under excitation of the 514 nm illumination, the top and the bottom Au clusters (the stars herein) both produce strong particle plasmons, gap plasmons and tip plasmons, as expected, in the theoretical discussion. Moreover, in the middle Si layer, strong plasmon near-field coupling can be observed for the upper and lower two layers. Particularly, the spatially displaced metal particles are also observed to provide strong spatial gap plasmon resonances. These features qualitatively demonstrate the potential plasmonic resonances and near-field coupling effects by this quasi-three-dimensional metal-semiconductor-metal resonant structure.

# 4 Conclusions

In summary, we proposed and demonstrated a quasi-three-dimensional plasmonic hotspots platform based on a metal-dielectric-metal triple layer structure. As for the ultra-thin silicon film buffered dual-layer Au clusters, the SERS signal was observed to be enhanced with a factor up to 735% in comparison with that of the system without the dielectric film. For the Au particles based SERS substrate, the Raman intensity showed a maximal enhancement factor of 503% when the silicon thin film was introduced for the quasi-three-dimensional layered structure. The SERS performance with a slight improvement was also achieved for the layered structures formed by the low-index silica film. Moreover, for the triple-layer Au clusters buffered with a silicon film, the SERS signal was observed to be as two to five times larger than that of the system with the low-index silica film. These features confirm a great advantage for the SERS performance by using an ultra-thin high-index dielectric film. In this metal-semiconductor-metal triple layer structure, the physical and chemical enhancements for the Raman scattering simultaneously exist. The metallic clusters or particles packed in proximity can produce strong plasmon resonances and near-field confinement, which can provide highly dense plasmonic hotspots in a three-dimensional scale. These resonant behaviors can lead to extremely enhanced Raman signals for the molecules. Besides the physical mechanism, the chemical effect can also be excited due to the ultra-thin silicon film, which is located between the upper and lower plasmonic nanostructures. The semiconductor material of silicon has a high density of electrons. In particular, the silicon film has a thickness close to the Bohr radius, which holds the capability of the electrons becoming excited, to interact with the other electronic oscillations. These features could therefore lead to the plasmon-like responses of the ultra-thin silicon film, and eventually provide a so-called charge transfer in the triple-layer SERS substrate. The findings not only show an alternative way to build an efficient SERS substrate in a large area at low-cost, but also provide novel insights on the semiconductor enhanced SERS technique.

**Acknowledgements:** This work was supported by the National Natural Science Foundation of China (NSFC) (11564017, Funder Id: http://dx.doi.org/10.13039/501100001809, 51761015, Funder Id: http://dx.doi.org/10.13039/501100001809, 11664015, Funder Id: http://dx.doi.org/10.13039/501100001809 and 11804134, Funder Id: http://dx.doi.org/10.13039/501100001809) and the Natural

Science Foundation of Jiangxi Province (2018ACB21005, Funder Id: http://dx.doi.org/10.13039/501100004479, 20182BCB22002, 20181BAB201015, Funder Id: http://dx.doi.org/10.13039/501100004479).

**Conflict of interest:** The authors declare no conflict of interest.

## References

[1] Fleischmann M, Hendra PJ, Mcquillan AJ. Raman spectra of pyridine adsorbed at a silver electrode. Chem Phys Lett 1974;26:163–6.
[2] Jeanmaire DL, Van Duyne RP. Surface Raman spectroelectrochemistry: Part I. Heterocyclic, aromatic, and aliphatic amines adsorbed on the anodized silver electrode. J Electroanal Chem 1977;84:1–20.
[3] Xu H, Bjerneld EJ, Käll M, Börjesson L. Spectroscopy of single hemoglobin molecules by surface enhanced Raman scattering. Phys Rev Lett 1999;83:4357.
[4] Kneipp K, Moskovits M, Kneipp H. Surface-enhanced Raman scattering: physics and applications. Heidelberg and Berlin, Germany: Springer, 2006.
[5] Nie SM, Emory SR. Probing single molecules and single nanoparticles by surface-enhanced Raman scattering. Science 1997;275:1102–6.
[6] Wang X, Zhu X, Shi H, et al. Three-dimensional-stacked gold nanoparticles with sub-5 nm gaps on vertically aligned $TiO_2$ nanosheets for surface-enhanced Raman scattering detection down to 10 fM scale. ACS Appl Mater Interfaces 2018;10:35607–14.
[7] Ozaki Y, Kneipp K, Aroca R. Frontiers of surface-enhanced Raman scattering: single nanoparticles and single cells. Hoboken, New Jersey, USA: John Wiley & Sons, Inc., 2014.
[8] Wang X, Zhu X, Chen Y, et al. Sensitive surface-enhanced Raman scattering detection using on-demand postassembled particle-on-film structure. ACS Appl Mater Interfaces 2017; 9:31102–10.
[9] Le Ru EC, Etchegoin PG. Single-molecule surface-enhanced Raman spectroscopy. Annu Rev Phys Chem 2012;63:65–87.
[10] Langer J, Novikov SM, Liz-Marzán LM. Sensing using plasmonic nanostructures and nanoparticles. Nanotechnology 2015;26:322001.
[11] Almaviva S, Botti S, Cantarini L, et al. Ultrasensitive RDX detection with commercial SERS substrates. J Raman Spectrosc 2014;45:41–6.
[12] Ben-Jaber S, Peveler WJ, Quesada-Cabrera R, et al. Photo-induced enhanced Raman spectroscopy for universal ultra-trace detection of explosives, pollutants and biomolecules. Nat Commun 2016;7:12189.
[13] Jiang T, Wang X, Zhou J, Jin H. The construction of silver aggregate with inbuilt Raman molecule and gold nanowire forest in SERS-based immunoassay for cancer biomarker detection. Sens Actuators B 2018;258:105–14.
[14] Zhang W, Fang Z, Zhu X. Near-field Raman spectroscopy with aperture tips. Chem Rev 2017;117:5095–109.
[15] Wei H, Xu H. Hot spots in different metal nanostructures for plasmon-enhanced Raman spectroscopy. Nanoscale 2013;5:10794-805.
[16] Li GC, Zhang Q, Maier SA, Lei D. Plasmonic particle-on-film nanocavities: a versatile platform for plasmon-enhanced spectroscopy and photochemistry. Nanophotonics 2018;7:1865–89.
[17] Maslovski SI, Simovski CR. Purcell factor and local intensity enhancement in surface-enhanced Raman scattering. Nanophotonics 2019;8:429–34.
[18] Jing J, Wang X, Li S, et al. Plasmonic nano-arrays for ultrasensitive bio-sensing. Nanophotonics 2018;7:1517–31.
[19] Yu M, Huang Z, Liu Z, et al. Annealed gold nanoshells with highly-dense hotspots for large-area efficient Raman scattering substrates. Sens Actuators B 2018;262:845–51.
[20] Lee SY, Hung L, Lang GS, Cornett JE, Mayergoyz ID, Rabin O. Dispersion in the SERS enhancement with silver nanocube dimers. ACS Nano 2010;4:5763–72.
[21] Hatab NA, Hsueh CH, Gaddis AL, et al. Free-standing optical gold bowtie nanoantenna with variable gap size for enhanced Raman spectroscopy. Nano Lett 2010;10:4952–5.
[22] Kravets VG, Zoriniants G, Burrows CP, et al. Cascaded optical field enhancement in composite plasmonic nanostructures. Phys Rev Lett 2010;105:246806.
[23] Osberg KD, Rycenga M, Harris N, et al. Dispersible gold nanorod dimers with sub-5 nm gaps as local amplifiers for surface-enhanced Raman scattering. Nano Lett 2012;12:3828–32.
[24] Gunnarsson L, Bjerneld EJ, Xu H, Petronis S, Kasemo B, Kall M. Interparticle coupling effects in nanofabricated substrates for surface-enhanced Raman scattering. Appl Phys Lett 2001;78:802–04.
[25] Cecchini MP, Turek VA, Paget J, Kornyshev AA, Edel JB. Self-assembled nanoparticle arrays for multiphase trace analyte detection. Nat Mater 2012;12:165–71.
[26] Kim NH, Hwang W, Baek K, et al. Smart SERS hot spots: single molecules can be positioned in a plasmonic nano-junction using host–guest chemistry. J Am Chem Soc 2018;140:4705–11.
[27] Tian Y, Shuai Z, Shen J, et al. Plasmonic heterodimers with binding site-dependent hot spot for surface-enhanced Raman scattering. Small 2018;14:e1800669, doi:10.1002/smll.201800669.
[28] Li JF, Huang YF, Ding Y, et al. Shell-isolated nanoparticle-enhanced Raman spectroscopy. Nature 2010;464:392–5.
[29] Liu F, Cao Z, Tang C, Chen L, Wang Z. Ultrathin diamond-like carbon film coated silver nanoparticles-based substrates for surface-enhanced Raman spectroscopy. ACS Nano 2010;4:2643–8.
[30] Zhao Y, Chu B, Zhang L, et al. Constructing sensitive SERS substrate with a sandwich structure separated by single layer graphene. Sens Actuators B 2018;263:634–42.
[31] Alessandri I, Lombardi JR. Enhanced Raman scattering with dielectrics. Chem Rev 2016;116:14921–81.
[32] Han XX, Ji W, Zhao B, Ozaki Y. Semiconductor-enhanced Raman scattering: active nanomaterials and applications. Nanoscale 2017;9:4847–61.

[33] Yilmaz M, Babur E, Ozdemir M, et al. Nanostructured organic semiconductor films for molecular detection with surface-enhanced Raman spectroscopy. Nat Mater 2017;16:918–24.
[34] Kuznetsov AI, Miroshnichenko AE, Brongersma ML, Kivshar YS, Luk'yanchuk B. Optically resonant dielectric nanostructures. Science 2016;354:aag2472.
[35] Feng T, Xu Y, Zhang W, Miroshnichenko AE. Ideal magnetic dipole scattering. Phys Rev Lett 2017;118:173901.
[36] Liu X, Chen J, Liu J, et al. III–V semiconductor resonators: a new strategy for broadband light perfect absorbers. Appl Phys Express 2017;10:111201.
[37] Xiang J, Jiang S, Chen JD, et al. Hot-electron intraband luminescence from GaAs nanospheres mediated by magnetic dipole resonances. Nano Lett 2017;17:4853–9.
[38] Bakker RM, Permyakov D, Yu YF, et al. Magnetic and electric hotspots with silicon nanodimers. Nano Lett 2015;15:2137–42.
[39] Limonov MF, Rybin MV, Poddubny AN, Kivshar YS. Fano resonances in photonics. Nat Photon 2017;11:543–54.
[40] Yang Y, Kravchenko II, Briggs DP, Valentine J. All-dielectric metasurface analogue of electromagnetically induced transparency. Nat Commun 2014;5:5753.
[41] Liu S, Keeler GA, Reno JL, Sinclair MB, Brener I. III–V semiconductor nanoresonators – A new strategy for passive, active, and nonlinear all-dielectric metamaterials. Adv Opt Mater 2016;4:1457–462.
[42] Cambiasso J, König M, Cortés E, Schlücker S, Maier SA. Surface-enhanced spectroscopies of a molecular monolayer in an all-dielectric nanoantenna. ACS Photonics 2018;5:1546 – 57.
[43] Taflove A, Hagness SC. Computational electrodynamics: the finite-difference time domain method. Norwood, MA: Artech House, Inc., 2005.
[44] Palik ED. Handbook of optical constants of solids I. Orlando: Academic Press, 1991.
[45] Huang Z, Chen J, Liu G, et al. Thermally generated metals for plasmonic coloring and surface-enhanced Raman sensing. Opt Eng 2018;57:037103.
[46] Maaroof AI, Cortie MB, Harris N, Wieczorek L. Mie and Bragg plasmons in subwavelength silver semi-shells. Small 2008;4:2292–9.
[47] Liu Z, Liu X, Huang S, et al. Automatically acquired broadband plasmonic-metamaterial black absorber during the metallic film-formation. ACS Appl Mater Interfaces 2015;7:4962–8.
[48] Yu M, Huang Z, Liu Z, et al. Annealed gold nanoshells with highly-dense hotspots for large-area efficient Raman scattering substrates. Sens Actuators B 2018;262:845–51.
[49] Voisin B, Salfi J, Bocquel J, Rahman R, Rogge S. Spatially resolved resonant tunneling on single atoms in silicon. J Phys: Condens Matter 2015;27:154203.
[50] Zhu W, Esteban R, Borisov AG, et al. Quantum mechanical effects in plasmonic structures with subnanometre gaps. Nat Commun 2016;7:11495.
[51] Allain A, Kang J, Banerjee K, Kis A. Electrical contacts to two-dimensional semiconductors. Nat Mater 2015;14:1195–205.
[52] Esfarjani K, Chen G, Stokes HT. Heat transport in silicon from first-principles calculations. Phys Rev B 2011;84:085204.
[53] Luoa T, Chen G. Nanoscale heat transfer-from computation to experiment. Phys Chem Chem Phys 2013;15:3389–412.
[54] Cahill DG, Braun PV, Chen G, et al. Nanoscale thermal transport. II. 2003–2012. Appl Phys Rev 2014;1:011305.
[55] Halas NJ, Lal S, Chang W-S, Link S, Nordlander P. Plasmons in strongly coupled metallic nanostructures. Chem Rev 2011;111:3913–61.
[56] Fang Z, Zhu X. Plasmonics in nanostructures. Adv Mater 2013;25:3840–56.
[57] Höflich K, Becker M, Leuchs G, Christiansen S. Plasmonic dimer antennas for surface enhanced Raman scattering. Nanotechnology 2012;23:185303.
[58] Yang L, Peng Y, Yang Y, et al. A novel ultra-sensitive semiconductor SERS substrate boosted by the coupled resonance effect. Adv Sci 2019;1900310.
[59] Zhang X, Zhang X, Luo C, et al. Volume-enhanced Raman scattering detection of viruses. Small 2019;15:1805516.
[60] Xiao Y-F, Zou C-L, Li B-B, et al. High-Q exterior whispering-gallery modes in a metal-coated microresonator. Phys Rev Lett 2010;105:153902.
[61] Liu Z, Liu G, Shao H, et al. Refractometric sensing of silicon layer coupled plasmonic–colloidal crystals. Mater Lett 2015;140:9–11.
[62] Willets KA, Van Duyne RP. Localized surface plasmon resonance spectroscopy and sensing. Annu Rev Phys Chem 2007;58:267–97.
[63] Yan W, Yang L, Chen J, Wu Y, Wang P, Li Z. In situ two-step photoreduced SERS materials for on-chip single-molecule spectroscopy with high reproducibility. Adv Mater 2017;29:1702893.
[64] Liang H, Li Z, Wang W, Wu Y, Xu H. Highly surface-roughened "Flower-like" silver nanoparticles for extremely sensitive substrates of surface-enhanced Raman scattering. Adv Mater 2009;21:4614–8.
[65] Hrelescu C, Sau TK, Rogach AL, et al. Selective excitation of individual plasmonic hotspots at the tips of single gold nanostars. Nano Lett 2011;11:402–7.
[66] Abbas A, Tian L, Morrissey JJ, Kharasch ED, Singamaneni S. Hot spot-localized artificial antibodies for label-free plasmonic biosensing. Adv Fun Mater 2013;23:1789–97.
[67] Zhang X, Xiao X, Dai Z, et al. Ultrasensitive SERS performance in 3D "sunflowerlike" nanoarrays decorated with Ag nanoparticles. Nanoscale 2017;9:3114.
[68] Mirshafieyan SS, Guo J. Silicon colors: spectral selective perfect light absorption in single layer silicon films on aluminum surface and its thermal tunability. Opt Express 2014;22:31545–54.
[69] Brongersma ML, Halas NJ, Nordlander P. Plasmon-induced hot carrier science and technology. Nat Nanotech 2015;10:25–34.
[70] Liu F, Hauger TC, Olsen BC, Luber EJ, Buriak JM. Plasmons, and patterns: mechanism of plasmon-induced hydrosilylation on silicon. Chem Mater 2016;28:9158–68.
[71] Kong L, Dasgupta B, Ren Y, et al. Evidences for redox reaction driven charge transfer and mass transport in metal-assisted chemical etching of silicon. Sci Rep 2016;6:36582.